PAPER

An exceptionally facile method to produce layered double hydroxides on a conducting substrate and their application for solar water splitting without an external bias†

Seungho Cho,‡[a] Ji-Wook Jang,‡[b] Yoon Bin Park,[c] Jae Young Kim,[b] Ganesan Magesh,[b] Jin Hyun Kim,[d] Minsu Seol,[c] Kijung Yong,[c] Kun-Hong Lee*[c] and Jae Sung Lee*[b]

An exceptionally facile process is presented for *in situ* formation of zinc chromium layered double hydroxide (ZnCr:LDH) nanosheets on a conducting substrate. Thus, ZnCr:LDH nanosheets were synthesized from a metallic Zn film/fluorine-doped tin oxide (FTO) glass by simply dipping into a Cr nitrate solution for only one minute at room temperature. Then, ZnCr:LDHs were converted into zinc chromium mixed metal oxide (ZnCr:MMO) nanoparticles by calcination. Under visible light irradiation (λ > 420 nm), the *in situ* synthesized ZnCr:MMO photoanode exhibited a stable and an order-of-magnitude higher activity for photoelectrochemical water splitting than that of a ZnCr:MMO film fabricated *ex situ* by electrophoretic deposition of already-synthesized ZnCr:MMO powders. More significant was that it generated anodic photocurrents even without an externally applied bias potential, which is an unprecedented result for an oxide photoanode-driven PEC system working under visible light.

Broader context

Photoelectrochemical (PEC) water splitting to hydrogen is an attractive method for capturing and storing solar energy in the form of chemical energy. Developing a method for large-scale fabrication of photoelectrodes for solar water splitting without an externally applied bias is still a challenge. In this paper, a facile process is presented for *in situ* formation of zinc chromium layered double hydroxide (ZnCr:LDH) nanosheets on a conducting substrate. Dipping Zn film/ fluorine-doped tin oxide glass into a chromium nitrate solution for one minute at room temperature produces ZnCr:LDH films that can be converted into zinc chromium mixed metal oxide (ZnCr:MMO) films by calcination. This *in situ* synthesized ZnCr:MMO photoanode exhibits a stable and an order-of-magnitude higher visible light PEC activity than that of a ZnCr:MMO film fabricated *ex situ* by electrophoretic deposition of already-synthesized ZnCr:MMO powders. The *in situ* ZnCr:MMO photoanode generates anodic photocurrents without an externally applied bias potential, which is an unprecedented result for an oxide photoanode-driven PEC system working under visible light. The method should be extendable to a wide range of combinations of metal oxides for solar water splitting systems.

1. Introduction

Hydrotalcite-like layered double hydroxides (LDHs) are an important class of ionic lamellar solids.[1] The LDHs have structures similar to the brucite structure, $Mg(OH)_2$, in which each Mg^{2+} ion is surrounded by six OH^- ions in an octahedral arrangement. They are obtained when a fraction of the divalent cations is isomorphously replaced by trivalent cations.[2,3] The

[a]*Department of Chemistry, Pohang University of Science and Technology (POSTECH), San 31 Hyoja-Dong, Pohang, 790-784 South Korea*

[b]*School of Energy and Chemical Engineering, Ulsan National Institute of Science and Technology (UNIST), 50 UNIST-gil, Ulsan, 689-798 South Korea. E-mail: jlee1234@ unist.ac.kr*

[c]*Department of Chemical Engineering, Pohang University of Science and Technology (POSTECH), San 31 Hyoja-Dong, Pohang, 790-784 South Korea. E-mail: ce20047@ postech.ac.kr*

[d]*School of Environmental Engineering, Pohang University of Science and Technology (POSTECH), San 31 Hyoja-Dong, Pohang, 790-784 South Korea*

† Electronic supplementary information (ESI) available: The XRD pattern of Zn-deposited FTO glass (Fig. S1). XRD patterns of Zn-deposited FTO glass with different Cr nitrate solution-dipping times (Fig. S2). The EDX pattern of particles detached from the substrate fabricated by the Cr nitrate solution-dipping process followed by calcination (Fig. S3). XRD patterns, photographs and synthesis procedures of ZnCr:LDH and ZnCr:MMO powders (Fig. S4). The photograph of the ZnCr:MMO/FTO glass fabricated by the Cr nitrate solution-dipping process followed by calcination (Fig. S5). Average photocurrent densities as a function of Zn thickness (Fig. S6) and dipping time (Fig. S7). Current–voltage curves under intermittent visible light irradiation for the ZnCr:LDH/Zn/FTO glass (Fig. S8). The current–time curve for the CoO_x-deposited ZnCr:MMO photoelectrode in a no-bias, two-electrode configuration with a Pt wire cathode (Fig. S9). The XRD pattern of a ZnCr:LDH/Zn substrate fabricated by immersing a Zn metal plate into Cr nitrate solution (Fig. S10). See DOI: 10.1039/c3ee43965h

‡ These authors contributed equally to this work.

This journal is © The Royal Society of Chemistry 2014

Energy Environ. Sci., 2014, 7, 2301–2307 | **2301**

higher charge of the trivalent cations generates an overall positive charge on the metal hydroxide layers, which is balanced by the intercalation of interlayer anions along with structural water. LDHs can accommodate a wide range of different anions and cations,[4–6] leading to a large compositional variety (the general formula: $[M^{2+}_{(1-x)}M^{3+}_{(x)}(OH)_2][anion_{x/m}{}^{m-}\cdot nH_2O]$ (M^{2+} = Zn^{2+}, Mg^{2+}, Co^{2+}, Ni^{2+}, Fe^{2+}, *etc.*; M^{3+} = Al^{3+}, Cr^{3+}, Ga^{3+}, Co^{3+}, Fe^{3+}, *etc.*)). These structures have a characteristic of the interspersion of cations on an atomic scale, thus no cation segregation occurs within a hydroxide layer.[4,7,8] Furthermore, LDHs can be readily converted into mixed metal oxide (MMO) structures with large surface areas by simple heat treatments, which are composed of homogeneously mixed two metal-oxide phases.[9,10]

In recent years, there has been a marked renewal of interest in photoelectrochemical (PEC) devices, which utilize charges generated within a light-absorbing semiconductor to split water or to reduce CO_2, allowing solar energy to be stored in chemical bonds and released in a clean, environmentally friendly manner.[11–13] Metal oxide semiconductors are promising materials for PEC applications, especially for the photoanode performing the oxidation half reaction due to their high stability in aqueous electrolytes and well-established synthesis procedures. Some LDHs (without conversion to MMOs) are reported to have photocatalytic activity for O_2 generation from water[14,15] and could be used for the photoanode materials in PEC devices. But their activity is usually low because limited thermal stability (stable only below 200 °C) makes the high temperature annealing unavailable to form highly crystalline LDHs. Hence, they are usually converted to MMOs by heat treatment above 500 °C. The MMOs derived from LDHs provide several advantages for the PEC applications; (i) a variety of compositional combinations inherited from a large compositional variety of LDHs, (ii) direct contact between homogeneously dispersed two metal-oxide phases, (iii) large surface areas, and (iv) ease of doping.[9,10,16,17]

For efficient solar energy conversion, photogenerated charge carriers should be transferred through constituents of photoelectrodes with minimal loss by recombination. Generally, photoelectrodes fabricated by post-deposition of already-synthesized particles on a conducting substrate exhibit a low charge carrier transfer efficiency between particles and at particles/conducting substrate interface (Fig. 1A). In contrast, *in situ* formation of photoactive materials on a conducting substrate provides better contact and favors facile photogenerated charge carrier transfer (Fig. 1B). In most cases reported to date, trivalent cations of LDHs synthesized *in situ* on the substrate are aluminum cations, *e.g.*, ZnAl:LDHs or MgAl:LDHs.[18] However, ZnAl:MMOs and MgAl:MMOs derived from these LDHs have wide band gaps and hence cannot absorb visible light. This is a serious impediment to the efficient use of solar energy because visible light accounts for 44–47% of the solar spectrum, whereas UV light makes up only 3–5%.

Herein, we report an exceptionally facile process for *in situ* formation of ZnCr:LDH nanosheets on a conducting substrate, fluorine-doped tin oxide (FTO) glass. Thus, ZnCr:LDH nanosheets were successfully synthesized by dipping a metallic Zn
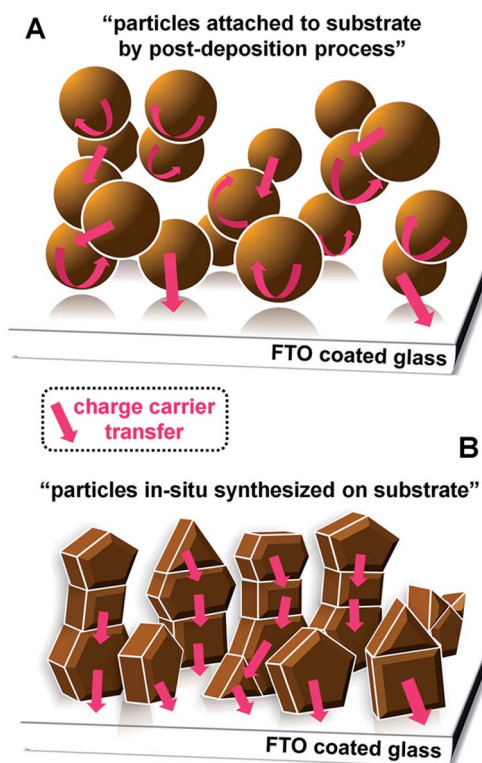

Fig. 1 Schematic diagram showing charge carrier transfer routes from (A) particles attached by the post-deposition process and (B) *in situ* synthesized particles to current-collecting substrates.

film on FTO into a Cr nitrate solution for only one minute at room temperature. This method is the easiest and simplest technique for synthesizing LDHs to the best of our knowledge. Then the ZnCr:LDH films were converted into ZnCr:MMO nanoparticle films by calcination in air at 527 °C. The *in situ* synthesized ZnCr:MMO photoanode exhibited an order of magnitude higher photocurrent density in photoelectrochemical water splitting under visible light irradiation than that of the ZnCr:MMO film *ex situ* fabricated by electrophoretic deposition of already-synthesized ZnCr:MMO powders. More significantly, from a practical point of view, it generated an anodic photocurrent without an externally applied potential. To the best of our knowledge, zero-bias water splitting is unprecedented in an oxide photoanode-driven PEC system working under visible light.

2. Results and discussion

2.1. Synthesis of ZnCr:LDHs on FTO by a simple solution dipping process and its conversion to ZnCr:MMOs

The most ingenious feature of the proposed method is the extreme simplicity and speed of the synthesis procedure for the ZnCr:LDH film. It is made by just dipping a Zn-deposited FTO glass in an aqueous solution of Cr nitrate at room temperature for only 1 minute. Fig. 2A shows an XRD pattern of the substrate after the solution-dipping process. The ZnCr:LDH (003) and (006) peaks were observed in addition to peaks for Zn metal and

2302 | *Energy Environ. Sci.*, 2014, **7**, 2301–2307

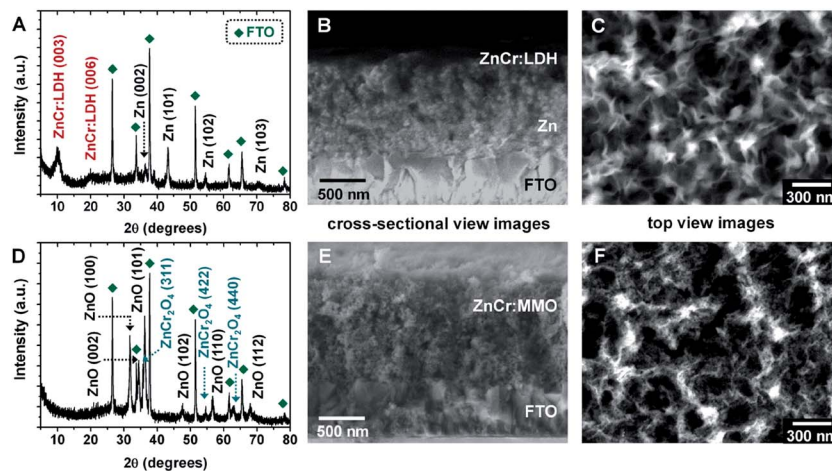This journal is © The Royal Society of Chemistry 2014

Fig. 2 (A) XRD pattern and (B and C) SEM images of Zn-deposited fluorine-doped tin oxide glass after the Cr nitrate solution-dipping process at room temperature for 1 min. (D) XRD pattern and (E and F) SEM images of the substrate after calcination at 527 °C in air for 2 h.

FTO. The XRD pattern before dipping shows only peaks of Zn metal and FTO (Fig. S1 of the ESI†). Fig. 2B displays a cross-sectional SEM image of the substrate after dipping. A dark ZnCr:LDH-rich layer was observed on the Zn film due to its lower electrical conductivity than those of Zn and FTO films. A top view SEM image (Fig. 2C) clearly shows ZnCr:LDH nanosheets. The quantities of LDHs synthesized on the substrates increased with dipping duration longer than 1 min (Fig. S2 in the ESI†). However, dipping for longer than 3 minutes caused exposure of FTO in some areas of the substrates by dissolution of Zn metal films into the dipping solution. To convert the ZnCr:LDH film to a ZnCr:MMO film, calcination was performed. After calcination, the ZnCr:LDH and Zn metal XRD peaks disappeared and new peaks emerged (Fig. 2D). These new peaks were indexed as ZnO (JCPDS no. 36-1451) and $ZnCr_2O_4$ (JCPDS no. 22-1107), indicating that ZnCr:MMOs made of ZnO and $ZnCr_2O_4$ phases were synthesized on the substrate. There was no other impurity phase detected. The nanosheet-like ZnCr:LDH morphology was changed to a random non-isotropic morphology of ZnCr:MMOs after calcination (Fig. 2E and F).

The synthesized film was detached by a knife from the calcined substrate and analyzed by TEM (Fig. 3). Fig. 3A displays a low-magnification TEM image of the detached structures on a holey carbon support. The EDX pattern (Fig. S3 in the ESI†) indicates that the structures are composed only of Zn, Cr, and O; the corresponding C and Cu signals are attributed to the carbon-coated copper mesh for the TEM analysis. The EELS elemental maps of the area demonstrate that Zn (Fig. 3B), Cr (Fig. 3C), and O (Fig. 3D) are distributed uniformly over the whole structure. A high-resolution TEM (HR-TEM) image (Fig. 3F) shows that the MMO nanostructures are made of highly crystalline ZnO and $ZnCr_2O_4$ phases as seen in the XRD pattern. The crystal grains of ~10 nm had lattice spacings of 0.25 nm and 0.28 nm, corresponding to the distance between the (311) planes in the $ZnCr_2O_4$ crystal lattice and that between the {100} planes in the ZnO crystal lattice, respectively. Taken together, SEM, XRD, TEM, EDX, and EELS data are consistent with the fact that a highly crystalline ZnCr:MMO film has been

successfully fabricated by the simple dipping-calcination process. HR-TEM analyses also demonstrate that the crystal grain interfaces are clean without noticeable defects or contamination which could become recombination sites for the photogenerated carriers. This feature would allow the *in situ* synthesized ZnCr:MMO film to have higher charge collection efficiencies compared to photoelectrodes prepared by post-synthesis assembly as discussed below.
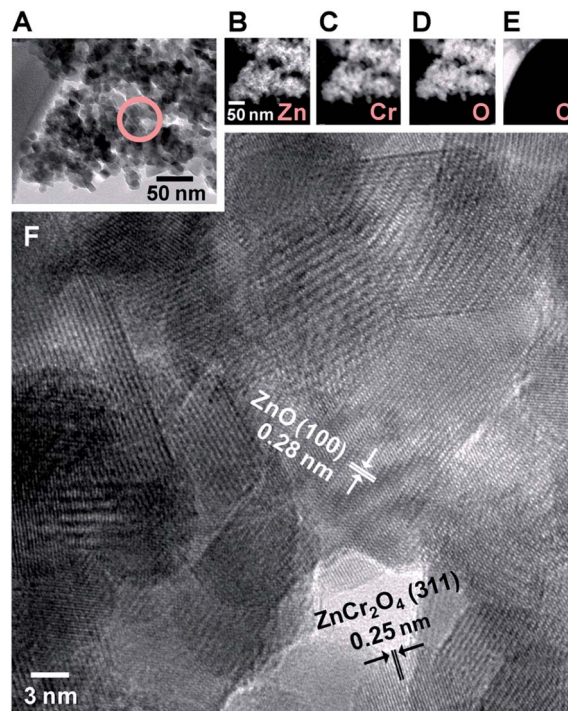

Fig. 3 (A) Low-magnification TEM image of the particles detached from the substrate fabricated by the Cr nitrate solution-dipping process followed by calcination at 527 °C in air for 2 h. (B–E) EELS elemental mappings of Zn, Cr, O and C, respectively. (F) HR-TEM image of the area indicated by the circle in (A).

Fig. 4 shows UV-vis diffuse reflectance spectra. Trace I is the spectrum of the ZnO film prepared by calcination of Zn-deposited FTO glass without the Cr nitrate solution-dipping process. The ZnO film exhibited a strong UV absorption band characteristic of the wide bandgap ZnO. The small tail extended to 520 nm in the absorption spectrum may be attributed to defects in the ZnO crystals. As a reference, ZnCr:LDH powders were synthesized according to the reported standard procedure,[14] and subsequent calcination at 527 °C in air for 2 h gave ZnCr:MMO powders that exhibited a visible light absorption characteristic of ZnCr:MMOs in trace III.[14,15] The XRD patterns and photographs of ZnCr:LDH and ZnCr:MMO powders are shown in Fig. S4 of the ESI.† Ttrace II shows the spectrum of the ZnCr:MMO film fabricated by calcination of the ZnCr:LDH film synthesized *in situ* on the substrate. It shows a wide range of visible light absorption. The (*in situ*) ZnCr:MMO film on FTO glass (Fig. S5 in the ESI†) exhibits an excellent transparency of the electrode. The transparency is essential to fabricate a tandem PEC cell with a photovoltaic device behind the photolysis cell to supply bias voltage using transmitted photons.[19] Hence, through the simple solution-dipping and calcination, only the UV-absorbing ZnO film turned to a ZnCr:MMO film absorbing ample visible light.

2.2. Photoelectrochemical water oxidation over ZnCr:MMO photoanodes

The film photoanodes were evaluated for their photoelectrochemical (PEC) water oxidation activity under intermittent visible-light irradiation ($\lambda > 420$ nm). The activity of the ZnCr:MMO photoanode depended on the initial Zn thickness that was controlled by the dipping time as shown in Fig. S6 and S7 in the ESI.† The optimum thickness of Zn was determined to be 1.5 µm obtained from dipping into the Cr nitrate solution for only 1 minute. Fig. 5A shows current–voltage (*I–V*) curves for the photoelectrodes. The ZnO film prepared by calcination of Zn-

Fig. 5 (A) Current–voltage curves in 0.2 M Na$_2$SO$_4$ solution (pH 6.5) under intermittent visible light irradiation ($\lambda > 420$ nm) for the ZnO photoelectrode fabricated by calcination at 527 °C in air for 2 h without the Cr nitrate solution-dipping process; the ZnCr:MMO photoelectrode *ex situ* synthesized and attached to a fluorine-doped tin oxide glass by an electrophoretic deposition method; the ZnCr:MMO photoelectrode fabricated by the Cr nitrate solution-dipping process followed by calcination at 527 °C in air for 2 h; CoO$_x$-deposited (*in situ*) ZnCr:MMO photoelectrode. (B) Current–voltage curves in 0.2 M Na$_2$SO$_4$ solution under intermittent visible light irradiation for the (*in situ*) ZnCr:MMO photoelectrode and CoO$_x$-deposited (*in situ*) ZnCr:MMO photoelectrode in a no-bias, two-electrode configuration with a Pt wire cathode. (C) Incident-photon-to-current-conversion efficiency (IPCE) measurements for ZnO and ZnCr:MMO photoelectrodes fabricated with and without the Cr nitrate solution-dipping process, respectively, carried out at 1.23 V *vs.* RHE in 0.2 M Na$_2$SO$_4$ solution. (D) Current–time curves of (*in situ*) ZnCr:MMO and CoO$_x$-deposited (*in situ*) ZnCr:MMO photoelectrodes kept at 1.23 V *vs.* RHE in 0.2 M Na$_2$SO$_4$ solution (pH 6.5).
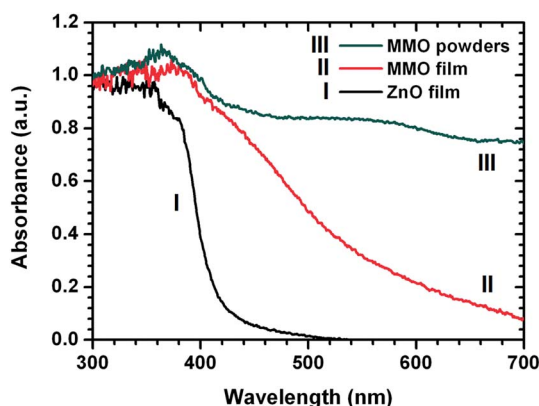
Fig. 4 UV-visible diffuse reflectance spectra of the ZnO film fabricated by calcination at 527 °C in air for 2 h without the Cr nitrate solution-dipping process (I), the (*in situ*) ZnCr:MMO film fabricated by the Cr nitrate solution-dipping process followed by calcination at 527 °C in air for 2 h (II), and the ZnCr:MMO powders derived from ZnCr:LDH powder synthesized by homogeneous precipitation followed by calcination at 527 °C in air for 2 h (III).
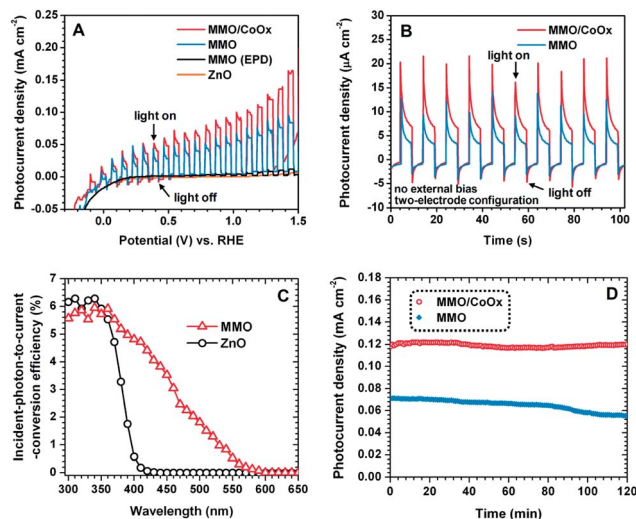
deposited FTO glass without solution-dipping showed a low photocurrent density of 2 µA cm^{-2} at 1.23 V *vs.* RHE under visible light irradiation, which is consistent with its wide band gap energy. The electrophoretically deposited ZnCr:MMO powders on FTO glass exhibited a photocurrent density of 7 µA cm^{-2} under the same conditions. On the other hand, the *in situ* synthesized ZnCr:MMO photoelectrode showed a greatly enhanced photocurrent density of 73 µA cm^{-2}. This current represents *ca.* 36 times increase from that of ZnO and *ca.* 10 times from that of the (*ex situ*) ZnCr:MMO photoelectrode. As mentioned, the duration of Cr nitrate solution-dipping was optimized as 1 min in the present study. The photocurrent increased when the dipping time increased from 30 s to 1 min (Fig. S7 in the ESI†). MoreZnCr:LDHs as precursors for ZnCr:MMOs were synthesized on the substrate after prolonged dipping time as shown in Fig. S2 in the ESI.† However, no further increase in photocurrent was detected when the dipping time increased from 1 to 2 min, indicating a saturation effect after 1 min. A linear sweep voltammogram was also obtained for a ZnCr:LDH/Zn/FTO glass before calcination to measure *I–V* characteristics of the LDH film (Fig. S8 in the ESI†). Its dark current onset potential on a highly cathodic region (~0.1 V *vs.*

2304 | *Energy Environ. Sci.*, 2014, **7**, 2301–2307

This journal is © The Royal Society of Chemistry 2014

RHE) and color change of the electrode indicate that the redox reaction of the electrode itself may occur unlike the stable operation of calcined electrodes.

The onset potential of the anodic photocurrent generated from the (*in situ*) ZnCr:MMO electrode prepared by the dipping-calcination method was approximately −0.1 V *vs.* RHE. This indicates that this *in situ* synthesized ZnCr:MMO film/FTO glass functions as a water oxidation photoanode under visible light irradiation, without an externally applied bias. The enhanced photocurrent density and the cathodic shift in the onset potential of the (*in situ*) ZnCr:MMO photoanode in comparison with the (*ex situ*) ZnCr:MMO photoanode demonstrate that the connection between particles and the electrode critically influences water oxidation efficiencies of the ZnCr:MMO photoanodes.

Cobalt-containing catalysts have emerged as particularly efficient and affordable co-catalysts for water oxidation.[20,21] When amorphous CoO_x was deposited on the MMO electrode,[20,22] the anodic photoresponse was further improved to 0.12 mA cm^{-2} at 1.23 V *vs.* RHE (Fig. 5A). The onset potential of dark current clearly shifted to the lower value (1.3 V *vs.* RHE) compared to the MMO electrode. These results indicate that CoO_x acts as an effective electrocatalyst for water oxidation on the photoanode. It is known that an oxygen evolution co-catalyst like CoO_x facilitates the transfer of charge carriers generated on the surface of the photoanode and lowers the overpotential of the water oxidation reaction. Photogenerated holes in the ZnCr:MMO films under visible light are promptly injected into the oxygen evolution cycle of CoO_x, which leads to efficient O_2 evolution with a reduced surface recombination probability.[23] The generated photocurrents are relatively small compared with common photoanodes like WO_3, Fe_2O_3, and $BiVO_4$ working only with a large applied bias potential (typically >1 V). However, Fig. 5B shows that the *in situ* synthesized ZnCr:MMO photoanode generated an anodic photocurrent upon visible light irradiation in the more practical 2-electrode configuration with a Pt wire cathode. Indeed, the visible light-induced water oxidation reaction can take place on the ZnCr:MMO photoanode without any energy input other than light energy. Fig. S9 in the ESI† shows that the photocurrent was sustained without an external bias under continuous visible light irradiation. To the best of our knowledge, the zero-bias water splitting is unprecedented in an oxide photoanode-driven PEC system, and it is highly desirable to produce solar hydrogen without external energy input.

2.3. Photoelectrochemical characterization

Incident-photon-to-current-conversion efficiency (IPCE) measurements were conducted to further study the photoresponse of the ZnCr:MMO photoanode as a function of the wavelength of incident light (Fig. 5C). The IPCE is defined by the following equation,

$$IPCE = [J \times 1240]/[P_{mono}\lambda] \qquad (1)$$

where J is the photocurrent density (mA cm^{-2}), P_{mono} is the light power density (mW cm^{-2}) at λ, and λ is the wavelength of incident light (nm). As expected, the ZnO film fabricated without the dipping process exhibited almost no photoresponse under visible light irradiation. The IPCE of the (*in situ*) ZnCr:MMO was significantly higher than that of the ZnO film under visible light illumination over the range 400–600 nm. The IPCE behavior of (*in situ*) ZnCr:MMO followed the UV-visible diffuse reflectance spectrum (Fig. 4(II)) qualitatively and the IPCE decreased with increasing wavelength, reaching almost zero at 600 nm. Discordance between the UV-vis diffuse reflectance spectrum and the IPCE data in the ranges of *ca.* 600–700 nm may be attributed to light scattering on the film.

To examine the initial stability of the photocurrent generated by the photoelectrodes, constant potential measurements were performed at 1.23 V *vs.* RHE in 0.2 M Na_2SO_4 solution (pH 6.5) (Fig. 5D). For the *in situ* synthesized ZnCr:MMO photoelectrode, an initial current density of 0.07 mA cm^{-2} at an applied potential of 1.23 V *vs.* RHE was obtained, which retained 79% of the initial current density after 2 h. In the case of the ZnCr:MMO/CoO_x film, a constant photocurrent level around 0.12 mA cm^{-2} was maintained for 2 h. In parallel with the PEC measurements, the amounts of evolved hydrogen were determined by gas chromatographic analysis. The stoichiometric H_2/O_2 gases evolved on working and counter electrodes, respectively. The amount of H_2 collected for 2 h was 2.95 μmol, which corresponds to about 90% of that expected by the net photocurrent (3.36 μmol) and the 90% represents the Faraday efficiency of this PEC system. These results indicate that the photoanodes fabricated by this method have a good stability and the photo-generated and collected charges are successfully used for water splitting, thus accomplishing a solar-to-hydrogen energy conversion. The CoO_x-deposited ZnCr:MMO photoelectrodes not only exhibited higher photoelectro-catalytic activity, but also showed better stability. The results strongly suggest that the deposited CoO_x suppresses the degradation of the photoelectrode by improving the selectivity of photogenerated holes toward water oxidation.

Electrochemical impedance spectroscopy (EIS) was also employed for investigation of the electrochemical behavior of photoelectrodes. The EIS measurements were conducted under the same conditions where semiconductors generated photocurrents to relate the impedance response directly to the physical processes responsible for the photocurrent generation.[24] Fig. 6 shows Nyquist plots of electrodes obtained from potentiostatic EIS. Here, x-axis represents the real part of the measured impedance and y-axis represents the negative number of the imaginary part of the measured impedance. The symbols in the plot represent experimental data and solid lines represent the result of fitting the data to an equivalent circuit model. To fit the measured EIS data, the Randles–Ershler model was adopted,[25] in which R_s is the electrolyte resistance, CPE is the capacitance phase element, and R_{ct} is the charge-transfer resistance of each electrode. The smaller value of R_{ct} and the larger value of CPE represent improved charge transport characteristics.[26] The charge-transfer resistance R_{ct} in *ex situ* MMO, *in situ* MMO and *in situ* MMO/CoO_x photoelectrodes was 317.5, 17.4 and 6.9 kΩ, respectively, and their simulated chemical capacitance CPE values were 10.6, 65.5, and 125.8 μF,

This journal is © The Royal Society of Chemistry 2014

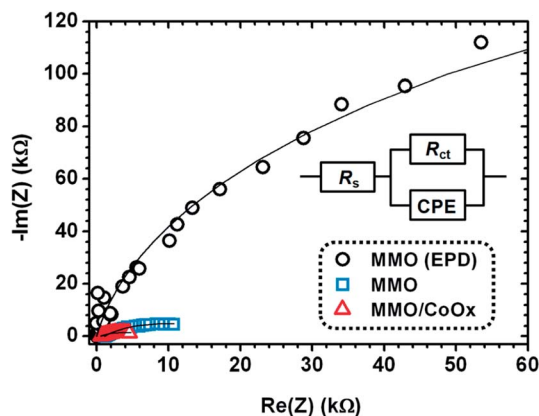*Energy Environ. Sci.*, 2014, **7**, 2301–2307 | **2305**

Fig. 6 Nyquist plots of electrochemical impedance spectroscopy results measured at 1.23 V *vs.* RHE in 0.2 M Na_2SO_4 solution. The inset shows an equivalent circuit for the photoanodes.

respectively. The fitted R_{ct} value and CPE value of the *in situ* MMOs were *ca.* 18 times smaller and *ca.* 6 times larger than those of the *ex situ* MMOs, which demonstrates the facilitated photogenerated charge carrier transfer in the *in situ* MMO photoanode. Better particle contact induced by the *in situ* MMO formation reduced not only the interparticle resistance but also the resistance across the MMO|FTO interface as illustrated in Fig. 1. The CoO_x deposition further reduced the R_{ct} value and increased the CPE value indicating that the loaded electrocatalyst induced efficient charge separation and transfer on the surface of MMOs.

Fig. 7 shows Mott–Schottky plots of ZnCr:MMO and ZnO photoelectrodes fabricated with and without Cr nitrate solution-dipping, respectively. Reversed sigmoidal plots were observed with an overall shape consistent with that of typical n-type semiconductors. A flat band potential (V_{fb}) of an electrode was determined by the Mott–Schottky relation,[27]

$$1/C^2 = (2/e\varepsilon\varepsilon_0 N)[V_a - V_{fb} - kT/e] \qquad (2)$$
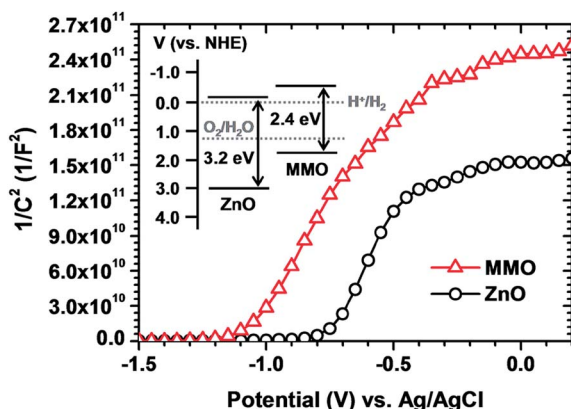

Fig. 7 Mott–Schottky plots of the ZnO and ZnCr:MMO photoelectrodes fabricated with and without the Cr nitrate solution-dipping process, respectively. The Mott–Schottky plots were measured in 0.2 M Na_2SO_4 solution (pH 6.5). The inset shows schematic band structures for ZnO and ZnCr:MMO.

where C is the space charge layer capacitance, e is the electron charge, ε is the dielectric constant, ε_0 is the permittivity of vacuum, N is the charge carrier density, and V_a is the applied potential. Thus, the V_{fb} values were determined by taking the x intercepts of linear fits to the Mott–Schottky plots, $1/C^2$, as a function of V_a; -1.07 V and -0.75 V *vs.* Ag/AgCl for the ZnCr:MMO and ZnO photoanodes, respectively. The V_{fb} of the ZnCr:MMO film was 320 mV more negative than that of the ZnO film. The band structures of ZnCr:MMO and ZnO are schematically compared in the inset of Fig. 7. This upward shift of the conduction band edge of the ZnCr:MMO system provides sufficient cathodic potential for hydrogen reduction from water,[28,29] resulting in the water oxidation reaction under visible light irradiation without an externally applied bias.

3. Conclusions

In summary, ZnCr:LDH nanosheets were successfully synthesized *in situ* on the conducting FTO substrate using an exceptionally facile process; by simply dipping the Zn film into a Cr solution for just one minute at room temperature. This method represents the easiest and simplest technique known to date for synthesizing LDHs. The ZnCr:LDH film on FTO was then converted to ZnCr:MMO upon calcination. In comparison with the ZnO film prepared by only calcination without dipping, the (*in situ*) ZnCr:MMO film exhibited greatly enhanced visible light absorption, and a 320 mV more negative flat band potential. In comparison with a ZnCr:MMO photoanode fabricated *ex situ* by electrophoretic deposition of already-synthesized ZnCr:MMO powders, the (*in situ*) ZnCr:MMO photoanode had higher charge collection efficiencies due to better contact between photoactive MMO particles and the conducting substrate, which was confirmed by the EIS analysis. Surprisingly, it was demonstrated in a more practical two-electrode configuration that the (*in situ*) ZnCr:MMO photoanode generated the anodic photocurrent upon visible light irradiation without any energy input other than light energy. However, there exists considerable room for improvement in the generation of MMO photoanodes by controlling the quantity, crystallinity and crystal grain sizes of MMO structures synthesized on the substrates. This simple method can be easily implemented on a large scale and can be applied to any substrate with Zn film or Zn metal foil (Fig. S10 in the ESI†). Therefore, the reported method should be extendable to a wide range of applications in which LDHs are key materials or their precursors.

4. Experimental details

Synthesis of ZnAl:LDH and ZnCr:MMO films

All chemicals used in this study were of analytical grade and used without further purification. Zn was deposited onto fluorine-doped tin oxide (FTO) glass (Pilkington, TEC 8, ~8 Ω per square) by sputtering. The Zn film-deposited FTO glass was immersed in an aqueous solution containing 0.6 M chromium nitrate nonahydrate $(Cr(NO_3)_3 \cdot 9H_2O)$ at room temperature for 1 min. The substrate was washed several times with deionized water and dried in an oven at 60 °C for 6 h. The ZnCr:LDH film

2306 | *Energy Environ. Sci.*, 2014, **7**, 2301–2307

This journal is © The Royal Society of Chemistry 2014

formed on the FTO substrate was placed in a furnace and maintained at 527 °C for 2 h in air for conversion into a ZnCr:MMO film/FTO glass.

Characterization

The morphology, crystallinity, chemical composition and optical properties of samples were determined using field-emission scanning electron microscopy (FESEM, JEOL JMS-7401F, operated at 10 keV), high-resolution scanning transmission electron microscopy (Cs-corrected HR-STEM, JEOL JEM-2200FS with an energy-dispersive X-ray spectrometer (EDX) and an electron energy loss spectrometer (EELS) operating at 200 kV, National Center of Nanomaterials Technology (NCNT)), X-ray diffraction (XRD, RIGAKU, D/MAX-2500/PC) and UV-vis diffuse reflectance spectroscopy (Shimadzu, UV2501PC).

Photoanode fabrication

Copper wires were attached on the as-prepared substrates with silver paste to make the electrical connections. The uncoated FTO surface was covered with epoxy resin. The co-catalyst CoO_x was deposited on a ZnCr:MMO film/FTO glass by illumination with a Hg lamp (450 W, Oriel) for 10 min in the 10 mM cobalt nitrate solution.

Photoelectrochemical (PEC) measurements

The current–potential (I–V) curves of PEC water oxidation were obtained in a 0.2 M Na_2SO_4 solution (pH 6.5) using a platinum foil counter electrode, a Ag/AgCl (3 M NaCl) reference electrode and a potentiostat (Potentiostat/Galvanostat Model 263A EG&G Princeton Applied Research). Prior to the measurement, the solution was purged with nitrogen for 30 min. The back side of photoanodes was illuminated with a 450 W Hg lamp (Oriel) attached with a UV cut-off filter ($\lambda > 420$ nm). The evolved amounts of H_2 and O_2 were analyzed using a gas chromatograph (HP5890) with a thermal conductivity detector and a molecular sieve 5-A column. Potentiostatic electrochemical impedance spectroscopy (EIS) was conducted at the DC potential 1.23 V $vs.$ RHE with the AC potential frequency range 5000–0.1 Hz under visible light irradiation ($\lambda > 420$ nm). Incident-photon-to-current-conversion efficiency (IPCE) was measured using the Hg lamp and a monochromator with a bandwidth of 5 nm. The IPCE was measured at 1.23 V $vs.$ RHE in a 0.2 M Na_2SO_4 solution (pH 6.5). Mott–Schottky analysis was carried out in the DC potential range −1.5 to +1.5 V $vs.$ Ag/AgCl with the AC potential frequency 5 kHz and the amplitude of AC potential 0.050 V under dark conditions in a 0.2 M Na_2SO_4 solution (pH 6.5).

Acknowledgements

References

1 V. Rives, *Layered Double Hydroxides: Present and Future*, Nova Science Publishers, Inc., New York, USA, 2001.

2 F. Cavani, F. Trifirò and A. Vaccari, *Catal. Today*, 1991, **11**, 173.

3 P. Beaudot, M. E. D. Roy and J. P. Besse, *Chem. Mater.*, 2004, **16**, 935.

4 P. J. Sideris, U. G. Nielsen, Z. Gan and C. P. Grey, *Science*, 2008, **321**, 113.

5 V. Rives and M. A. Ulibarri, *Coord. Chem. Rev.*, 1999, **181**, 61.

6 A. I. Khan and D. O'Hare, *J. Mater. Chem.*, 2002, **12**, 3191.

7 O. Clause, B. Rebours, E. Merlen, F. Trifirò and A. Vaccari, *J. Catal.*, 1992, **133**, 231.

8 M. Bellotto, B. Rebours, O. Clause, J. Lynch, D. Bazin and E. Elkaïm, *J. Phys. Chem.*, 1996, **100**, 8527.

9 M. Bellotto, B. Rebours, O. Clause, J. Lynch, D. Bazin and E. Elkaïm, *J. Phys. Chem.*, 1996, **100**, 8535.

10 X. Zhao, F. Zhang, S. Xu, D. G. Evans and X. Duan, *Chem. Mater.*, 2010, **22**, 3933.

11 S. R. Pendlebury, A. J. Cowan, M. Barroso, K. Sivula, J. Ye, M. Grätzel, D. R. Klug, J. Tang and J. R. Durrant, *Energy Environ. Sci.*, 2012, **5**, 6304.

12 N. S. Lewis and D. G. Nocera, *Proc. Natl. Acad. Sci. U. S. A.*, 2006, **103**, 15729.

13 M. G. Walter, E. L. Warren, J. R. McKone, S. W. Boettcher, Q. Mi, E. A. Santori and N. S. Lewis, *Chem. Rev.*, 2010, **110**, 6446.

14 S. Cho, J.-W. Jang, K.-j. Kong, E. S. Kim, K.-H. Lee and J. S. Lee, *Adv. Funct. Mater.*, 2013, **23**, 2348.

15 X. Zhao, L. Wang, X. Xu, X. Lei, S. Xu and F. Zhang, *AIChE J.*, 2012, **58**, 573.

16 X. Guo, F. Zhang, D. G. Evans and X. Duan, *Chem. Commun.*, 2010, **46**, 5197.

17 C. G. Silva, Y. Bouizi, V. Fornés and H. García, *J. Am. Chem. Soc.*, 2009, **131**, 13833.

18 J. L. Gunjakar, T. W. Kim, H. N. Kim, I. Y. Kim and S.-J. Hwang, *J. Am. Chem. Soc.*, 2011, **133**, 14998.

19 O. Khaselev and J. Turner, *Science*, 1998, **280**, 425.

20 Y.-H. Lai, C.-Y. Lin, Y. Lv, T. C. King, A. Steiner, N. M. Muresan, L. Gan, D. S. Wright and E. Reisner, *Chem. Commun.*, 2013, **49**, 4331.

21 V. Artero, M. Chavarot-Kerlidou and M. Fontecave, *Angew. Chem., Int. Ed.*, 2011, **50**, 7238.

22 Y. Tak and K. Yong, *J. Phys. Chem. C*, 2008, **112**, 74.

23 D. K. Zhong and D. R. Gamelin, *J. Am. Chem. Soc.*, 2010, **132**, 4202.

24 E. A. Ponomarev and L. M. Peter, *J. Electroanal. Chem.*, 1995, **396**, 219.

25 J. E. Randles, *Discuss. Faraday Soc.*, 1947, **1**, 11.

26 W. J. Jo, J.-W. Jang, K.-j. Kong, H. J. Kang, J. Y. Kim, H. Jun, K. P. S. Parmar and J. S. Lee, *Angew. Chem., Int. Ed.*, 2012, **51**, 3147.

27 F. Cardon and W. P. Gomes, *J. Phys. D: Appl. Phys.*, 1978, **11**, L63.

28 M. Radecka, M. Rekas, A. Trenczeck-Zajac and K. Zakrzewska, *J. Power Sources*, 2008, **181**, 46.

29 Y. J. Hwang, A. Boukai and P. Yang, *Nano Lett.*, 2009, **9**, 410.

This journal is © The Royal Society of Chemistry 2014

Energy Environ. Sci., 2014, **7**, 2301–2307 | **2307**